Received: 10 March 2021 | Revised: 1 July 2021 | Accepted: 10 July 2021

DOI: 10.1111/cas.15057

ORIGINAL ARTICLE

Cancer Science WILEY

Immune infiltration profiling in gastric cancer and their clinical implications

Feifei Ren[1,2,3] | Qitai Zhao[2,4] | Minghai Zhao[5] | Shaogong Zhu[6] | Bin Liu[1,2,3] | Ihtisham Bukhari[1] | Kai Zhang[2,4] | Wanqing Wu[7] | Yuming Fu[7] | Yong Yu[3] | Youcai Tang[8] | Pengyuan zheng[1,2,3] | Yang Mi[1,2,3]

[1]Key Laboratory of *Helicobacter pylori*, Microbiota and Gastrointestinal Cancer of Henan Province, Marshall Medical Research Center, Fifth Affiliated Hospital of Zhengzhou University, Zhengzhou, China

[2]Academy of Medical Science, Zhengzhou University, Zhengzhou, China

[3]Department of Gastroenterology, Fifth Affiliated Hospital of Zhengzhou University, Zhengzhou, China

[4]Biotherapy Center, First Affiliated Hospital of Zhengzhou University, Zhengzhou, China

[5]Department of Gastrointestinal Surgery, Henan Cancer Hospital, Affiliated Cancer Hospital of Zhengzhou University, Zhengzhou, China

[6]Department of Gastrointestinal Surgery, People' s Hospital of Zhengzhou University, Zhengzhou, China

[7]Department of Gastrointestinal Surgery, Fifth Affiliated Hospital of Zhengzhou University, Zhengzhou, China

[8]Department of Pediatrics, Fifth Affiliated Hospital of Zhengzhou University, Zhengzhou, China

Correspondence
Yang Mi and Pengyuan Zheng, The Fifth Affiliated Hospital of Zhengzhou University, Zhengzhou, China.
Emails: miyang198@126.com (YM); medp7123@126.com (PZ)

Funding information
National Key Research and Development Program in China, Grant/Award Number: 2020YFC2006100; Excellent Foreign Scientist Studio of Henan Province in China, Grant/Award Number: GZS2018001; Zhengzhou Major Collaborative Innovation Project, Grant/Award Number: 18XTZX12003; key projects of discipline construction in Zhengzhou University, Grant/Award Number: XKZDJC202001; medical service capacity improvement project of Henan Province in China, Grant/Award Number: Yu Wei Medicine [2017] No. 66.

Abstract

The abundance and type of immune cells in the tumor microenvironment (TME) significantly influence immunotherapy and tumor progression. However, the role of immune cells in the TME of gastric cancer (GC) is poorly understood. We studied the correlations, proportion, and infiltration of immune and stromal cells in GC tumors. Data analyses showed a significant association of infiltration levels of specific immune cells with the pathological characteristics and clinical outcomes of GC. Furthermore, based on the difference in infiltration levels of immune and stromal cells, GC patients were divided into two categories, those with "immunologically hot" (hot) tumors and those with "immunologically cold" (cold) tumors. The assay for transposase-accessible chromatin using sequencing and RNA sequencing analyses revealed that the hot and cold tumors had altered epigenomic and transcriptional profiles. Claudin-3 (CLDN3) was found to have high expression in the cold tumors and negatively correlated with $CD8^+$ T cells in GC. Overexpression of CLDN3 in GC cells inhibited the expression of MHC-I and CXCL9. Finally, the differentially expressed genes between hot and cold tumors were utilized to generate a prognostic model, which predicted the overall

Abbreviations: ATAC-seq, assay for transposase-accessible chromatin using sequencing; CLDN3, claudin 3; DEG, differentially expressed gene; GC, gastric cancer; GO, Gene Ontology; HSC, hematopoietic stem cell; KEGG, Kyoto Encyclopedia of Genes and Genomes; NK, natural killer; OS, overall survival; PD-1, programmed death 1; PD-L1, programmed death-ligand 1; PFS, progression-free survival; PPI, protein-protein interaction; RNA-seq, RNA sequencing; ROC, receiver operating characteristic; ssGSEA, single-sample Gene Set Enrichment Analysis; TCGA, The Cancer Genome Atlas; Tcm, central memory T cell; Tem, effector memory T cell; Th1/Th2, T helper 1/2 cell; TME, tumor microenvironment; Treg, regulatory T cell.

Feifei Ren, Qitai Zhao, and Minghai Zhao contributed equally to this work.

survival of GC as well as patients with immunotherapy. Overall, we undertook a comprehensive analysis of the immune cell infiltration pattern in GC and provided an accurate model for predicting the prognosis of GC patients.

KEYWORDS
ATAC, gastric cancer, immune infiltration, predicting model, RNA-seq

1 | INTRODUCTION

Gastric cancer is the third leading cause of cancer-related deaths worldwide. Gastric cancer has no effective treatment, so surgical resection is the only option; however, the success rate is only 60% and unfortunately most patients with advanced disease do not undergo surgical resection.[1,2] Clinical trials of immune checkpoint inhibitors PD-1 and PD-L1 have shown that disease progression is inhibited in many cancers, including GC, but the clinical response was observed in a small subset of patients and many patients failed to respond.[3-5] Therefore, it is crucial to elucidate the relevant mechanisms of tumor progression to improve the immunotherapy response in GC patients. The tumor immunomicroenvironment is the most important factor for studying immunotherapy response, which is usually classified into two phenotypes, noninflamed and immune-inflamed tumors. Noninflamed tumors have two subtypes, immune-excluded and immune desert phenotypes. These two phenotypes could reflect the absence of pre-existing antitumor immunity.[6] Several studies have reported that the immune-inflamed and noninflamed phenotypes could be relevant in response to immune checkpoint inhibitors.[7,8] Therefore, converting a noninflamed into immune-inflamed tumor is necessary for therapeutic approaches.

In the current study, we applied xCell, ssGSEA, and TIMER tools to quantify the comprehensive tumor immune milieu of GC patients. Considering the difference in immune response as an essential driver of the GC progression and response to treatment, we classified GC tumors into "immunologically hot" (hot) and "immunologically cold" (cold) tumors, then ATAC-seq and RNA-seq were used to determine their differences. We further identified target genes that regulate immune cell infiltration in the TME. In addition, based on the DEGs between hot and cold tumors, we constructed a model for predicting the OS of GC and patients treated with immunotherapy.

2 | MATERIALS AND METHODS

2.1 | Data acquisition

The RNA-seq data and clinical information of the GC patients were obtained from the UCSC Cancer Browser. For the immunotherapeutic efficiency analysis, three transcriptomic datasets from patients with metastatic urothelial cancer treated with anti-PD-L1 agents (atezolizumab; http://research-pub.gene.com/IMvigor210CoreBiologies/), patients with melanoma treated with anti-PD-1 agents (nivolumab; Gene Expression Omnibus, GSE91061), and patients with metastatic melanoma treated with anti-PD-1 agents (pembrolizumab or nivolumab; Gene Expression Omnibus, GSE78220) were downloaded.[9-11] The sequencing data of ATAC was downloaded from the NCI website (https://gdc.cancer.gov/about-data/publications/ATACseq-AWG).[12]

2.2 | Immune estimation

A total of 64 immune and stromal cells were calculated using the R package "xCELL"; samples with $P < .05$ were selected for further analysis.[13,14] Next, 34 immune cells containing markers were calculated using the R package "GSVA".[15] The six tumor-infiltrating immune cell types were downloaded from TIMER.[16] The immune score, stromal score, and tumor purity were calculated using the R package "ESTIMATE".

2.3 | Analysis of DEGs

Based on the immune score and immune cell infiltration level, the samples were divided into hot and cold tumors. The R package "limma" was used to calculate DEGs with criteria as follows: |logFC|>1 and adjusted *P* value <.05.

2.4 | Functional enrichment analysis and PPI network

All DEGs with a *P* value (adjusted *P* value) less than .05 were analyzed for function prediction through KEGG and GO. In addition, the PPI network of overlapping DEGs with |logFC|>1 was obtained from STRING then reconstructed by Cytoscape.

2.5 | Construction of prediction model

The RNA-seq data of GC tumors with survival information of the patients were randomly divided into training and testing cohorts using the R package "caret" then univariate survival analysis was undertaken on the DEGs. Furthermore, LASSO analysis was carried out using R package "glmnet" and for optimization of the prediction model a stepwise proportional hazards model was used.

2.6 | Survival analysis

To undertake survival analysis of the immune and stromal cells, samples were divided into two groups. The log-rank test was used to determine the significant effect of the cells on OS and PFS of patients with GC. Survival analysis was undertaken using R package "survival" and ROC curves were analyzed by "survivalROC".

2.7 | Immunohistochemistry analysis

The GC tissue specimens were harvested, fixed in 10% buffered formalin, sectioned, and stained with anti-CLDN3 (1:50; #16456-1-AP; Proteintech) and anti-CD8α (D8A8Y) (1:200; #85336; Cell Signaling Technology). Based on the intensity of both nuclei and membrane staining (0, blank; 1, light yellow; 2, yellow; and 3, brown) and the extent of stained cells (0, <10%; 1, 10%-40%; 2, 40%-70%; and 3, >70%), each specimen was assigned a score and calculated by multiplying two items into a total score (range, 0-9).

2.8 | Cell culture

The human gastric cancer cell lines SGC7901 and AGS were purchased from the Institute of Biochemistry and Cell Biology of the Chinese Academy of Sciences. All cells were cultured in RPMI-1640 medium supplemented with 10% FBS at 37°C and 5% CO_2 in a humidified incubator.

2.9 | Quantitative real-time PCR

Total RNA was extracted from GC tissues and cells (AGS and SGC7901) using TRIzol (TaKaRa) and cDNA was synthesized by a reverse transcription kit (Toyobo). The quantitative PCR was carried out using the QuantiNova SYBR Green PCR kit (Qiagen) and a set of specific primers (Table S1). Relative gene expression was calculated by the $2^{-\Delta\Delta Ct}$ method.

2.10 | Plasmids and transfection

The full cDNA of human *CLDN3* was amplified by PCR and cloned into the mammalian expression vector pcDNA3.1-myc-His. Gastric cancer cells were transfected CLDN3-pcDNA3.1-myc-His (OE-CLDN3) using Lipofectamine 2000.

2.11 | Western blotting

The cells were lysed in RIPA lysis buffer (Solarbio) containing proteinase inhibitors (Sigma-Aldrich) and total protein was quantified by BCA electrophoresed using 12% SDS-PAGE gels. Blots were transferred to a PVDF membrane, blocked with 5% skimmed milk, and incubated with anti-CLDN3 (1:1000, #ab214487; Abcam), and anti-β-Actin (1:1000, #3700; Cell Signaling Technology) Abs overnight at 4°C. The following day, membranes were washed and incubated with secondary Abs for 1 hour and detected with an enhanced chemiluminescence reagent.

2.12 | Immunofluorescence

The cells were cultured on coverslips for 24 hours, fixed in 4% PFA for 15 minutes, then blocked with blocking buffer (PBS-T, 3% BSA) for 30 minutes and incubated with HLA class I ABC polyclonal Ab (1:50, #15240-1-AP; Proteintech) for 1 hour at room temperature. Cells were washed and stained with corresponding secondary Ab for 1 hour at room temperature. Finally, a mounting medium containing DAPI was dropped on the slide for nuclear staining and images were taken by confocal microscope.

2.13 | Enzyme-linked immunosorbent assay

Cells were transfected with the OE-CLDN3 plasmid and 48 hours later stimulated by γ-interferon and tumor necrosis factor -α (50 ng/ml each) (PeproTech) as previously described.[17] After incubating for 24 hours, media were harvested, and ELISA was undertaken for CXCL9 and CXCL10 using the ELISA kits (Lianke Bio). All samples were assessed in triplicate.

2.14 | Statistical analysis

All the statistical analyses were carried out with the R and GraphPad software packages. The χ^2 test was used for studying correlations between immune infiltration and pathological parameters. Wilcoxon's test was used to compare the infiltration of immune cells in normal and tumor tissues, as well as in hot and cold tumors. Analysis of variance was used to compare the immune score, stromal score, and tumor purity among the three clusters. For the survival analysis, *P* values were calculated using the log-rank test. A *P* value of less than .05 was considered statistically significant.

3 | RESULTS

3.1 | Immune landscape related to histopathological characteristics of GC

To explore the effect of infiltrating cells on the malignancy of GC, we determined the association between different immune cell subsets and GC pathological characteristics. For this purpose, the RNA-seq data of 341 GC patients from TCGA database were obtained and the score of cells calculated using xCell (Figures 1 and

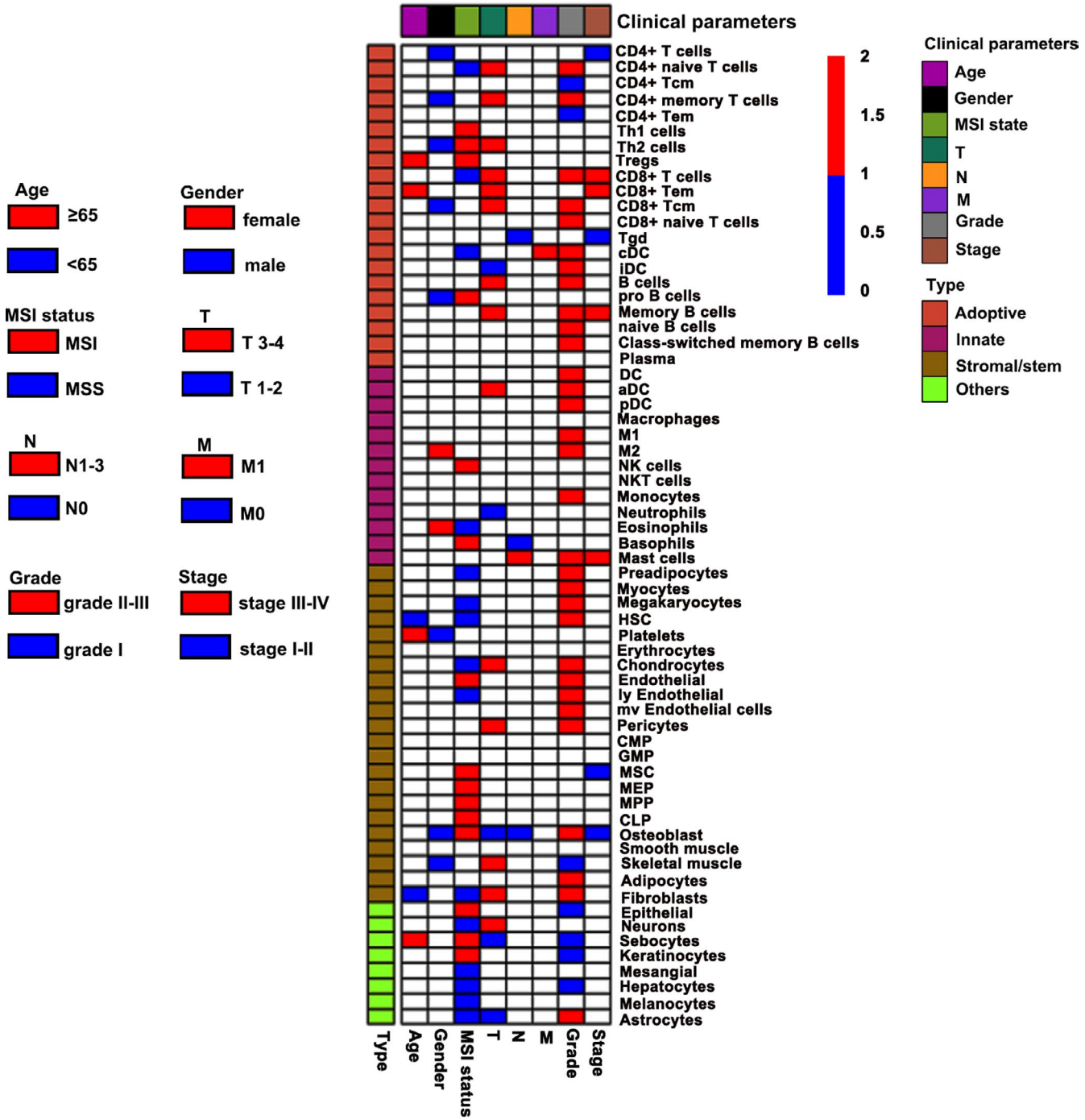

FIGURE 1 Landscape of immune and stromal cell types infiltrating the tumor microenvironment of gastric cancer. Heatmap showing the correlation of 64 types of infiltrating cells (columns) and clinical parameters (rows). Cells with red and blue indicate a significant difference; white indicates no significant difference. cDC, conventional dendritic cell; CLP, common lymphoid progenitor; CMP, common myeloid progenitor; DC, dendritic cell; GMP, granulocyte-monocyte progenitor; iDC, immature dendritic cell; MEP, megakaryocyte-erythrocyte progenitor; MPP, multipotent progenitor; MSC, mesenchymal stem cell; NK, natural killer; Tcm, central memory T cell; Tem, effector memory T cell; Tgd, gamma delta T cell; Th1/Th2, T helper 1/2 cell; Treg, regulatory T cell

S1). Elevated levels of Tregs, $CD8^+$ Tems, platelets, and sebocytes, and decreased levels of HSCs and fibroblasts were detected in older patients. Gender-based analysis showed higher levels of immune effector cells ($CD4^+$ T cells, $CD4^+$ memory T cells, and $CD8^+$ Tcm) in male patients. Of note, $CD8^+$ T cells and memory B cells increased in patients with higher T stage, grade, and advanced pathological stage. In addition, tumors with microsatellite instability had significantly higher proportions of Th1, Th2, pro-B, NK, and endothelial cells, basophils, and Tregs. Overall, infiltration levels of specific immune cells showed association with the pathological characteristics of GC, suggesting that they play a vital role in regulating the progression of GC.

3.2 | Prognostic associations of subsets of infiltrating cells

Considering the critical role of the composition of infiltrating cells in prognosis, we further investigated their association with survival of GC. The results showed that pro-B, Th1, megakaryocyte-erythroid progenitor, NK, Treg, and $CD4^+$ memory T cells were associated with favorable OS and PFS. In contrast, skeletal muscle, HSC, astrocytes, fibroblasts, adipocytes, neurons, chondrocytes, megakaryocytes, and hepatocytes were associated with poor OS and PFS (Figures 2 and S2). Our data indicated that specific immune cells were related to the prediction of clinical outcomes.

3.3 | Immune-based subtyping of GC tumors

To further explore the patterns of cell infiltration in TME, we grouped the GC patients into different categories and evaluated the correlations between infiltrated immune cells. The results revealed that immune cells infiltrated in the TME coexisted, and $CD8^+$

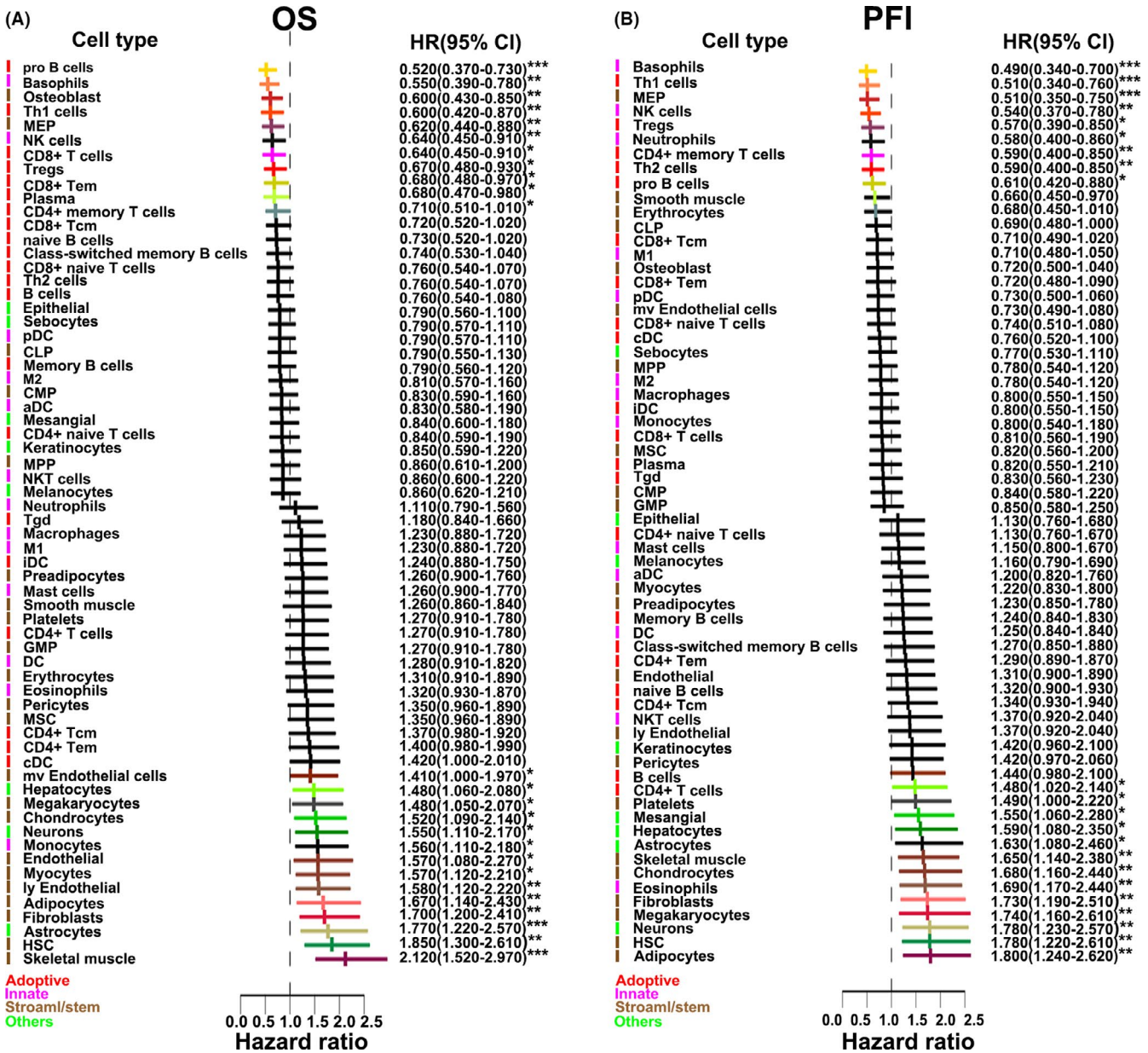

FIGURE 2 Prognostic associations of subsets of immune cells in Cox regression analysis. Forest plots showing the association between each immune cell subset and survival in The Cancer Genome Atlas total dataset. A, Overall survival (OS). B, Progression-free survival (PFS). Unadjusted hazard ratios (HR) are shown with 95% confidence intervals (CI). aDC, activated dendritic cell; cDC, conventional dendritic cell; CLP, common lymphoid progenitor; CMP, common myeloid progenitor; DC, dendritic cell; GMP, granulocyte-monocyte progenitor; HSC, hematopoietic stem cell; iDC, immature dendritic cell; MEP, megakaryocyte-erythrocyte progenitor; MPP, multipotent progenitor; NK, natural killer; pDC, plasmacytoid dendritic cell; Tcm, central memory T cell; Th1/Th2, T helper 1/2 cell; Treg, regulatory T cell. *$P < .05$, **$P < .01$, ***$P < .001$

T cells were strongly correlated with Th cells, dendritic cells, and macrophages (Figure 3A). Surprisingly, immune-suppressive Tregs and M2 macrophages were also positively correlated with immune cells, indicating an immunosuppressive microenvironment induced by tumor cells. Additionally, stromal cells showed a negative correlation with immune cells; this extracellular organization could inhibit the infiltration of immune cells in TME. Furthermore, hierarchical clustering of the major types of the cells identified three clusters. Immunocytes and antigen-presenting cells were significantly higher in cluster 1, whereas cluster 2 and 3 had comparatively low numbers of immune cells (Figure 3B). Patients displaying a high immune response signature had significantly improved OS rate (cluster 1 vs. cluster 2) (Figure S3). The different immune regulatory molecules showed a high expression pattern in patients from cluster 1 to cluster 3 (Figure 4); however, CD276 showed an opposite expression trend.

3.4 | Validation of tumor classification by ssGSEA and TIMER tool

Based on the genes expressed in all three clusters, we defined clusters 1 and 2 as hot tumors and cluster 3 as cold tumors. We precisely analyzed the differential distributions of immune cells in the two groups estimated by ssGSEA (Figure 5A) and TIMER tool (Figure 5B) in hot and cold tumors. The results showed that the hot tumors had high infiltration levels of immune cells, whereas the cold tumors had relatively low levels of immune cells. The consistency between the immune profiles in different computational algorithms verified the reliability of our classification method.

3.5 | Different chromatin accessibility of hot and cold tumors

Based on the median immune scores, we evaluated the changes in chromatin accessibility between hot and cold tumors by dividing samples into immunologically hot and cold groups (Figure 6A). A total of 766 differentially expressed genes showing substantial chromatin remodeling function were identified from the ATAC-seq data of hot and cold tumors (Figure 6B). Hot tumors showed altered epigenomic profiles characterized by upregulation of immunoregulatory genes specifically involved in antigen presentation (Figure 6C,E). However, the regions that were more accessible in cold tumors were associated with cancer-related signaling pathways such as I-κB kinase/nuclear factor-κB signaling and cell-cell junction organization (Figure 6D,F).

3.6 | Transcriptome analysis revealed differences in molecular mechanisms of hot and cold tumors

To gain further insight into the molecular features of hot and cold tumors, we undertook a global transcriptome analysis (Figure 7A), and hierarchical cluster analysis showed hot tumors were relatively well separated from cold tumors (Figure 7B). Differentially expressed genes in cold and hot tumors were chosen for GO and KEGG analyses. The top

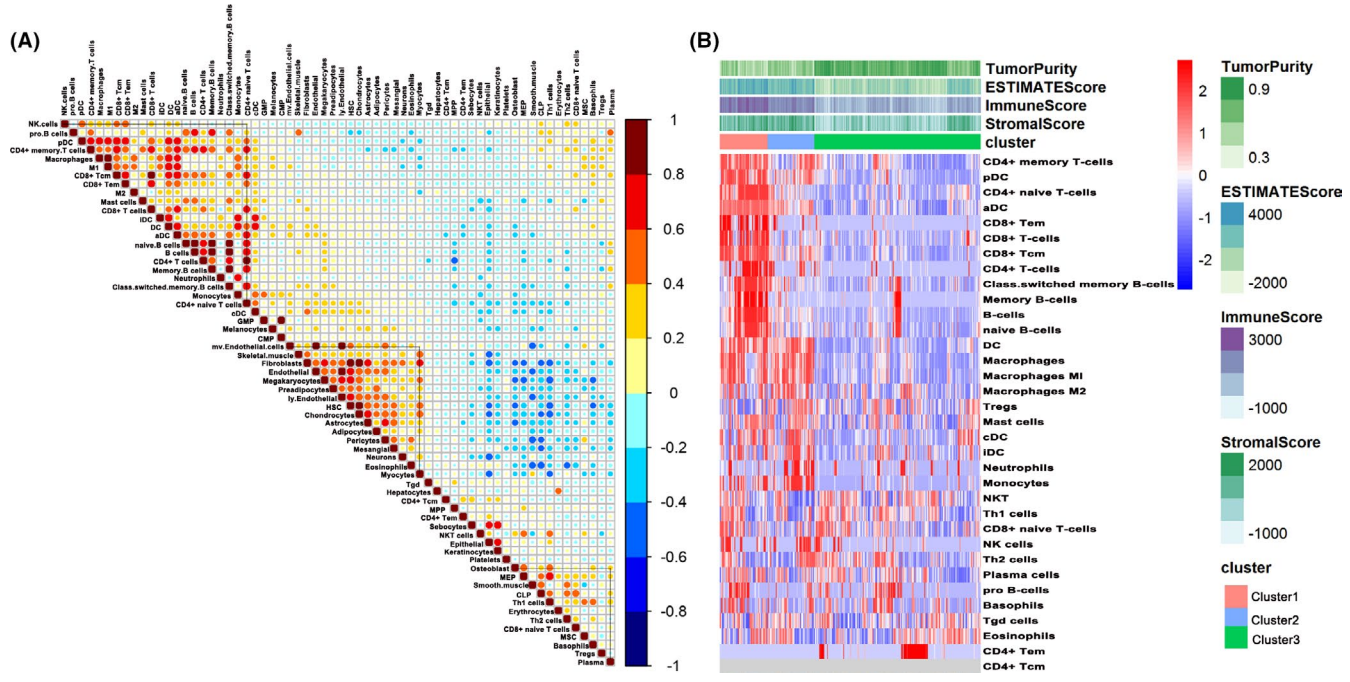

FIGURE 3 Clustering gastric cancer patients. A, Correlation heatmap depicting correlations between infiltrating cells in tumor. B, Distribution of 34 types of cells in three clusters. aDC, activated dendritic cell; cDC, conventional dendritic cell; DC, dendritic cell; iDC, immature dendritic cell; NK, natural killer; pDC, plasmacytoid dendritic cell; Tcm, central memory T cell; Tem, effector memory T cell; Tgd, gamma delta T cell; Th1/Th2, T helper 1/2 cell; Treg, regulatory T cell

10 upregulated genes in cold tumors (Table 1) were mainly involved in the Wnt signaling pathway, Rap1 signaling pathway, and tight junctions; however, upregulated genes in hot tumors were related to immune response (Figure 7C-F). Furthermore, we constructed a PPI network of DEGs and identified the top 20 hub genes mainly expressed in hot tumors; these genes were mainly Th1 like chemokines and receptors, including CXCL9, CCL5, and CCR5. In contrast, only two genes, *NOTUM* and *CEACAM6*, were expressed in cold tumors (Figure 7G).

3.7 | *CLDN3* is positively correlated with immunosuppressive function in GC

To identify novel immune-related therapeutic targets in GC, we evaluated the relationship between gene expression and immune infiltration. Among the top 10 upregulated genes in cold tumors (Table 1), *CLDN3* was negatively correlated with immune cells (Figure 7H), specifically highly significantly negatively related with $CD8^+$ T cells (Figure S4). Furthermore, wet lab analysis confirmed this strong negative correlation between *CLDN3* and $CD8^+$ T lymphocyte infiltration in tumor tissues (Figure 8A,B). Gastric cancer tissues with high expression of *CLDN3* showed decreased levels of $CD8^+$ T cells, and showed negative correlation with CD8A, CXCL9, and CXCL10 (Figure 8E-H). *CLDN3* had low endogenous expression in GC cell lines SGC7901 and AGS (Figure 9A), therefore, we overexpressed *CLDN3* in SGC7901 and AGS cells (Figure 9B-D), which did not affect the biological function of the GC cells (Figure S6). Further investigation in CLDN3 overexpressed cells showed downregulation of MHC class I, which is required for $CD8^+$ T cell antigen recognition (Figure 9C-H). We also found a decreased level of CXCL9 in the *CLDN3* overexpressed cells. Of note, a positive correlation between the expression of CXCL9 and CD8A levels was observed in the TCGA dataset and inhouse GC tumor samples.

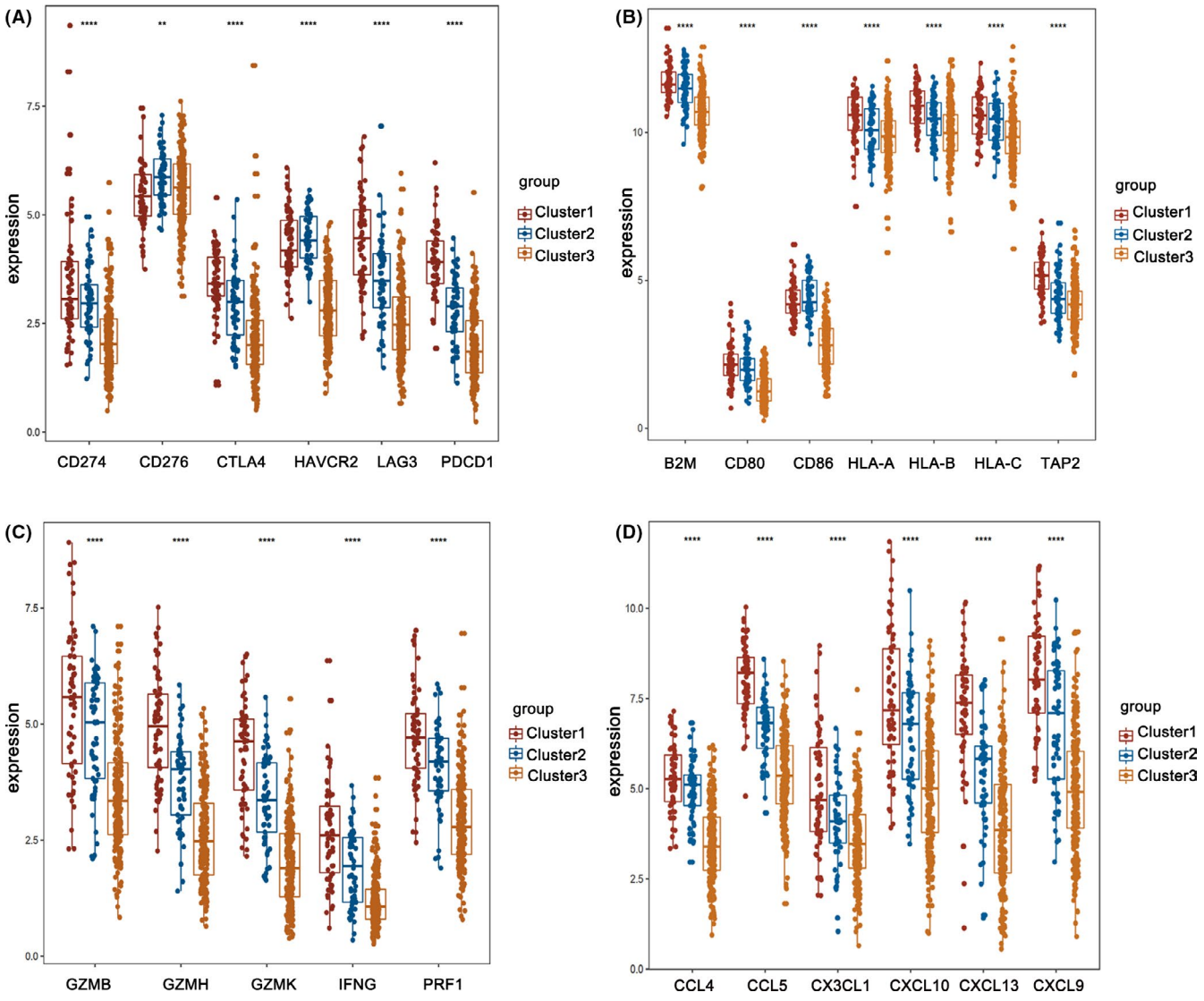

FIGURE 4 Different immune characteristics of the clusters. A-D, Comparison of (A) co-inhibitory molecules, (B) MHC antigen presentation-related molecules, (C) cellular immune killer molecules, and (D) T cell-attracting chemokines, and gene expression levels among the clusters

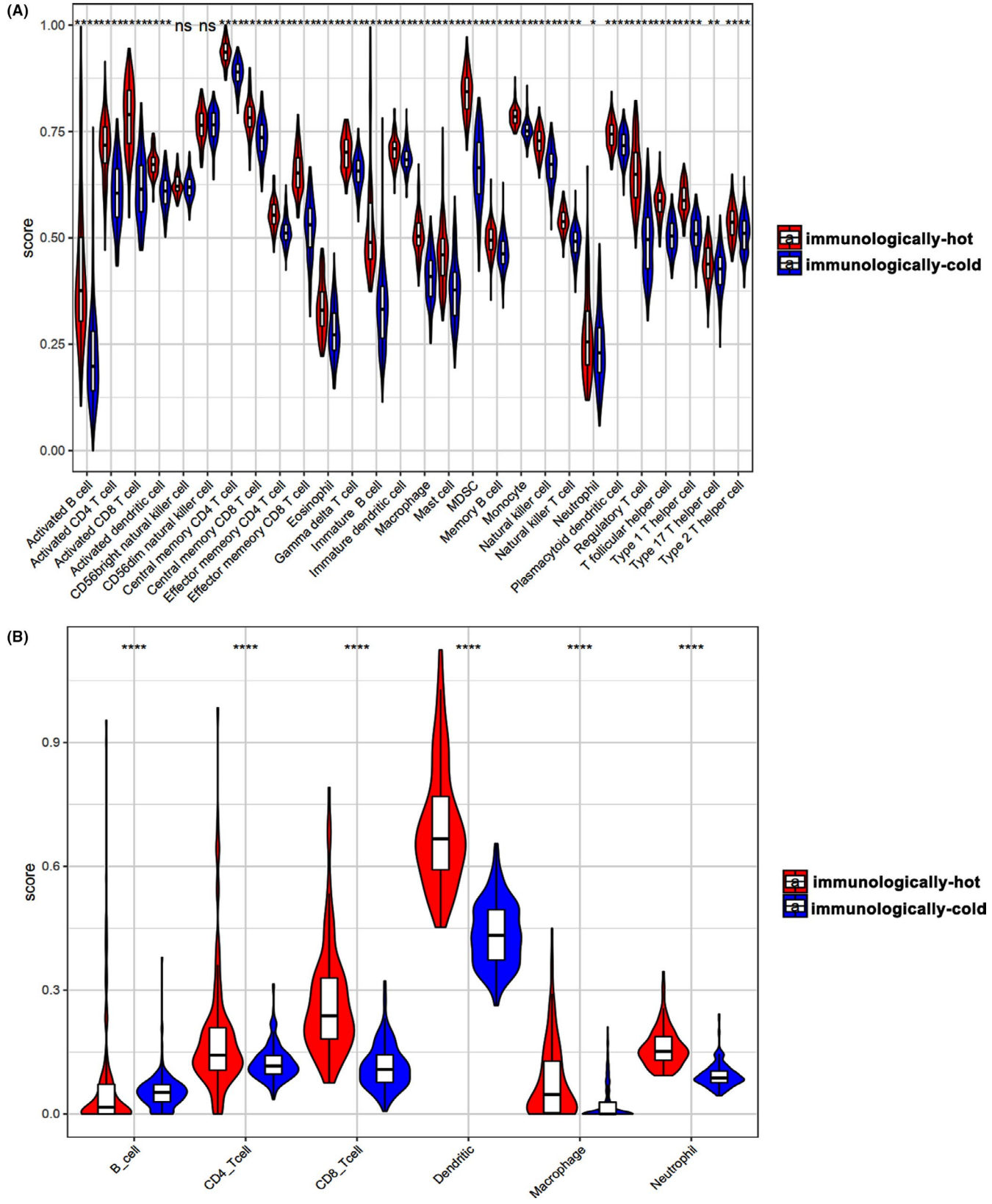

FIGURE 5 Violin plot comparing the proportions of immune cells between hot and cold tumor samples using (A) single-sample Gene Set Enrichment Analysis and (B) TIMER tool. Horizontal and vertical axes represent immune cells and relative percentages, respectively. Red and blue represent hot and cold tumor samples, respectively. Data were assessed using the Wilcoxon rank-sum test. MDSC, myeloid-derived suppressor cell; ns, not significant

3.8 | Construction and validation of a prediction model for OS

To comprehensively assess the relationship between immune-related genes and tumor recurrence in patients with GC, we first undertook a univariate analysis using DEGs and then used a LASSO regression model to select the best combination of the genes' sets (Figure 10A,B). To determine whether this model contained only the most predictive genes, a stepwise Cox proportional hazards regression model was applied, which identified a final set of 14 genes (Figure 10C). In the TCGA training cohort, patients were assigned to the high-risk group and low-risk group based on the optimized risk value (Figure 10D). Kaplan-Meier survival analyses showed that patients with a high-risk score had an unfavorable survival (Figure 10E, $P < .0001$). To evaluate the predictive performance, we calculated the time-dependent area under the ROC curves. The results showed that the areas under the curves for the risk model in predicting 2-, 3-, 4-, and 5-year survival were 0.769, 0.805, 0.83, and 0.829, respectively (Figure 10F), which indicates a good capability for predicting OS in patients using the 14-gene combination. Moreover, we explored whether our prediction model could predict the immunotherapeutic benefits. Surprisingly, the Kaplan-Meier curve (Figure 10G-I) revealed that the high-risk group was associated with unfavorable survival in patients who received immunotherapy.

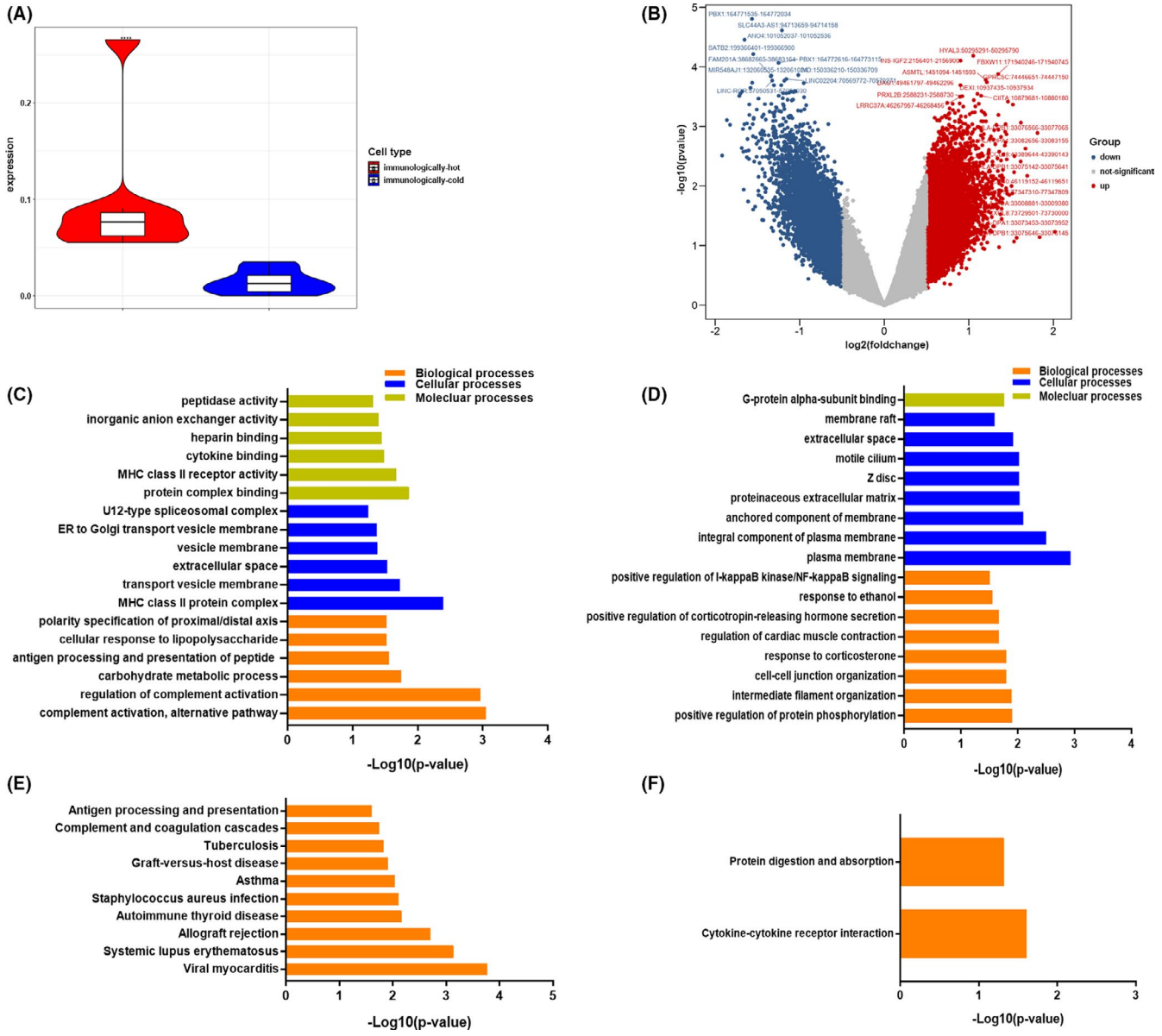

FIGURE 6 Changes in chromatin accessibility between hot and cold tumors. A, Violin plot showed the immune score between the two groups. B, The volcano plot shows the different peaks of gene expression between the two groups identified by assay for transposase-accessible chromatin with sequencing. Gene Ontology and Kyoto Encyclopedia of Genes and Genomes pathway enrichment analysis of more open chromosome regions in the (C, E) hot tumors and (D, F) cold tumors

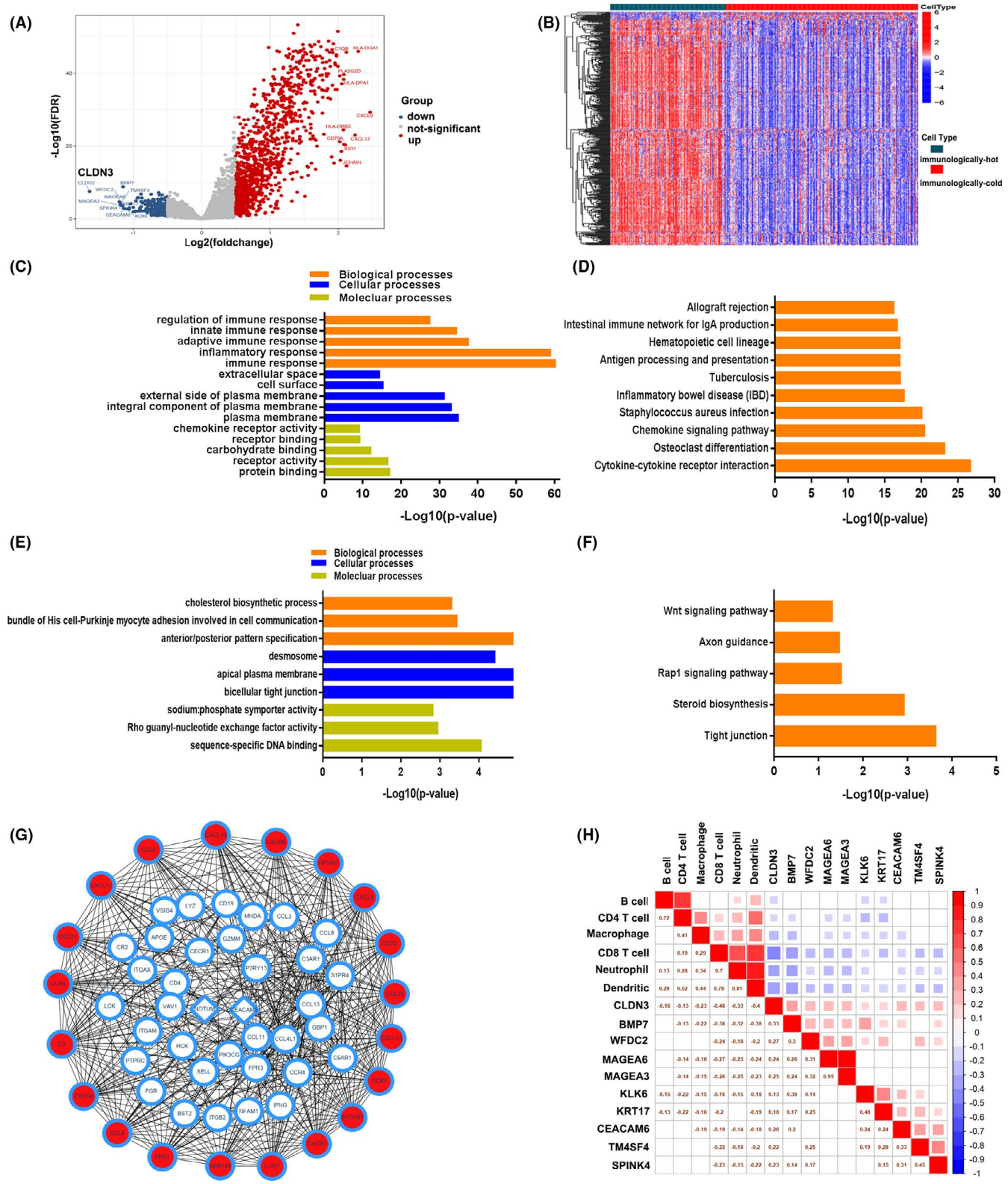

FIGURE 7 Comparison of gene expression profile for hot and cold tumors. A, Volcano plot for differentially expressed genes between hot and cold tumors. Red shows high and blue shows lower expressing genes in hot tumors. B, Heatmap of commonly upregulated or downregulated differentially expressed genes (DEGs) in hot and cold tumors. Gene Ontology and Kyoto Encyclopedia of Genes and Genomes pathway analysis of (C, D) upregulated DEGs and (E, F) downregulated DEGs. G, Interaction network of the DEGs. Circle and diamond nodes represent upregulated and downregulated DEGs, respectively. Red nodes represent hub genes. H, Correlation analysis of the top 10 upregulated genes and six immune cells

4 | DISCUSSION

Immune checkpoint inhibitors that block the PD-1/PD-L1 pathway can induce durable and robust responses in patients with various cancers, including GC.[3-5] However, clinical responses only occur in a subset of patients. Immunotherapy concentrates on the activation of immunologic molecular components to defend against cancer cells in the TME. Thus, it is essential to deeply explore the influence of the TME on GC immunotherapy.

In this study, we discovered the levels of $CD4^+$ naive T cells, $CD4^+$ memory T cells, $CD8^+$ T cells, $CD8^+$ Tcm, B cells, and memory B cells increased with tumor progression. Possibly, advanced tumors might have more mutations in the genome than early-stage tumors, and the more mutation-related neoantigens (targets of tumor immunity) can activate more T cells and produce a stronger immune response. In the TME, stromal cells express a large number of surface and secretory molecules, which directly inhibit $CD4^+$ and $CD8^+$ T cells, and activate immunosuppressed myeloid cells.[18,19] We also found poor prognosis of most of the stromal cells in the TME, and the stromal cells are negatively correlated with most of the immune cells, indicating that the presence of stromal cells might affect the infiltration of immune cells. Natural killer cells are the crucial component of the innate immune system that can produce inflammatory cytokines and destroy malignant cells.[20,21] The current study showed that infiltration of NK cells had a positive correlation with $CD8^+$ Tcm and $CD8^+$ Tem, and also associated with prolonged OS and PFS, indicating their protective role in GC development. CD4 memory T cells are the Th cells, but also assist many other types of cells and act as a catalyst, increasing immune protection through many different pathways.[22] Our results also revealed that high infiltration of CD4 memory T cells was associated with improved treatment outcomes. Eosinophils are related to angiogenesis and metastasis, and elevated eosinophil levels are associated with poor prognosis.[23,24] Our study is in agreement with previous research showing that eosinophils are associated with poor PFS. However, xCELL has some limitations, such as detecting unrelated cells. In the current study, we analyzed 64 cells by xCELL. Based on differential expression of the genes, xCELL detected some unrelated cells like osteoblasts, chondrocytes, sebocytes, and hepatocytes. To overcome this issue, we applied other tools like ssGSEA and TIMER and successfully validated the results.

Our study also found that GC was distinctly separated into immunogenic and immune-resistant subtypes; based on the infiltration of 34 immune cells, we classified GC into three clusters. Clusters 1 and 2 had an abundance of immune cells, antigen-presenting cells, and immune regulatory molecules, suggesting a pre-existing antitumor immune response. In contrast, cluster 3 had low numbers of immune cells, MHC molecules, and immune regulatory molecules. We defined clusters 1 and 2 as the hot tumors and cluster 3 as the cold tumors. We then revealed the differential mechanism of hot and cold tumors at the genomic and transcriptome levels.

CD276, also known as B7-H3, a member of the B7 superfamily, was previously known to inhibit T cell activation and autoimmunity.[25,26] We found significantly high expression of CD276 in cold tumors, which is different from other immune checkpoint molecules (Figure 4A), suggesting its role as an alternative therapy for immune checkpoints in patients not responding to PD-1/PD-L1 treatment.

To explore the differential mechanism of hot and cold tumors, ATAC-seq showed that more accessible regions in hot tumors were

TABLE 1 Top 10 upregulated genes in cold tumors

Gene symbol	|Log FC|	*P* value	Function
CLDN3	1.64	1.45E-09	Involved in tight junction-specific obliteration of the intercellular space
MAGEA6	1.21	1.78E-06	Enhances ubiquitin ligase activity of RING-type zinc finger-containing E3 ubiquitin-protein ligases
TM4SF4	1.19	5.15E-06	Regulates the adhesive and proliferative status of intestinal epithelial cells
MAGEA3	1.19	1.78E-05	Enhances ubiquitin ligase activity of RING-type zinc finger-containing E3 ubiquitin-protein ligases
WFDC2	1.16	2.44E-05	Broad range protease inhibitor
BMP7	1.15	6.94E-11	Induces cartilage and bone formation
SPINK4	1.14	0.000156	Includes serine-type endopeptidase inhibitor activity
CEACAM6	1.12	0.000197	Involved in cell adhesion and tumor progression
KLK6	1.11	0.000235	Includes serine-type endopeptidase activity and peptidase activity
KRT17	1.07	0.000313	Regulates protein synthesis and epithelial cell growth

Abbreviation: FC, fold change.

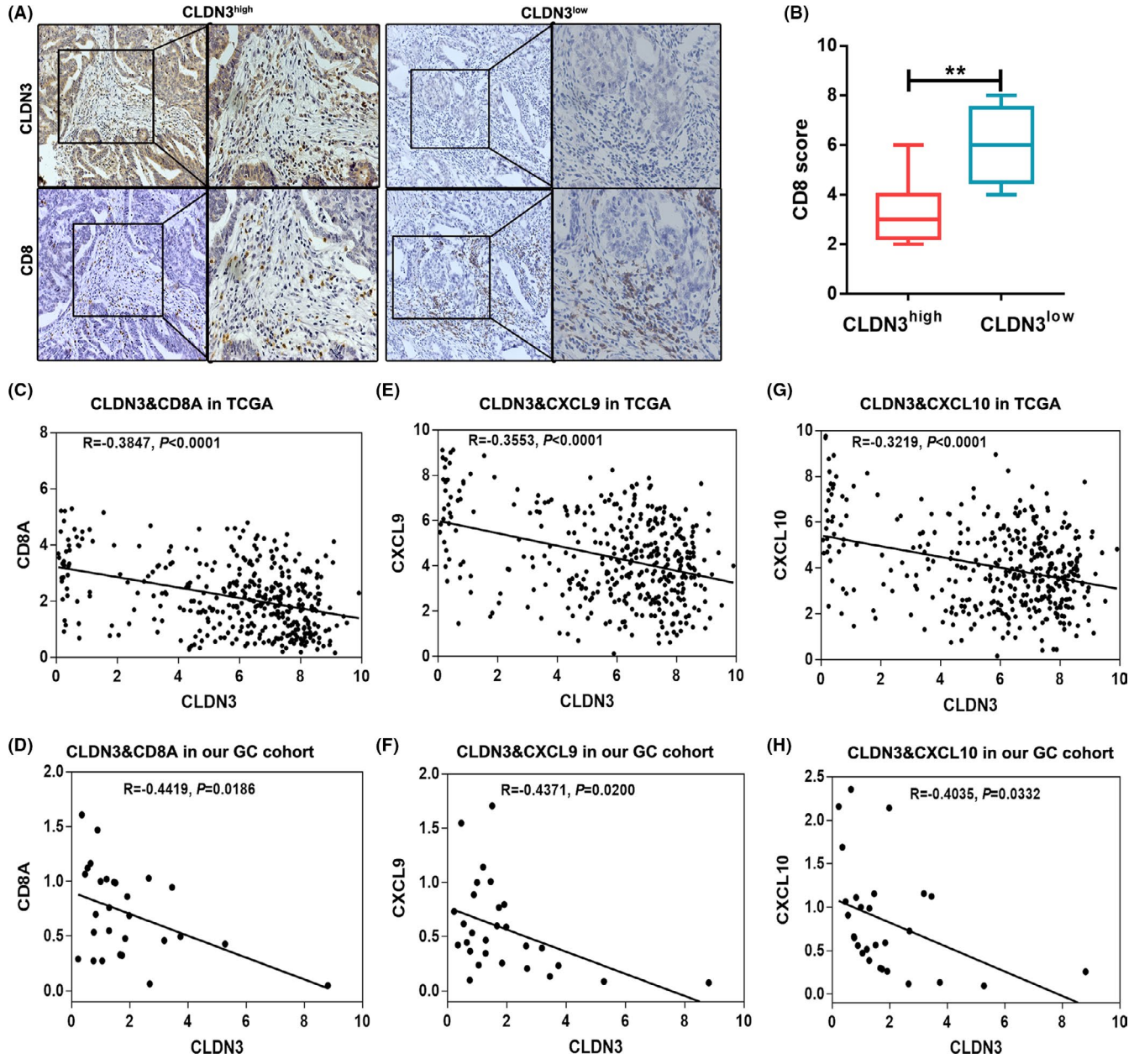

FIGURE 8 Correlation between claudin 3 (CLDN3) and $CD8^+$ T cells in gastric cancer (GC) samples. A, Immunohistochemical (IHC) staining for CLDN3 and CD8, showing high (left panel) and low (right panel) expression levels of CLDN3 (n = 20). B, IHC score of CLDN3 and CD8 in GC tumors. C, E, G, Correlation analysis CLDN3 with (C) CD8A, (E) CXCL9, and (G) CXCL10 expression in The Cancer Genome Atlas (TCGA) database. D, F, H, Correlation analysis of CLDN3 with (D) CD8A, (F) CXCL9, and (H) CXCL10 in patient-derived GC samples (n = 28)

associated with important immunoregulatory genes and key immune pathways. However, the cold tumors displayed upregulation of cancer-related signaling pathways that could be regulated by chromatin remodeling.

Furthermore, we undertook GO and KEGG pathway enrichment analyses on DEGs obtained from the RNA-seq analysis to uncover the differential mechanism of hot and cold tumors at the transcriptome level, which revealed that hot tumors were enriched with immune-related signaling and cold tumors showed enrichment of cancer-related signaling pathways, such as the Wnt signaling pathway, Rap1 signaling pathway, and tight junctions. Protein-protein interaction results identified 20 hub genes in the hot tumors, which were mainly related to immunity. However, the only two hub genes in cold tumors, *CEACAM6* and *NOTUM*, contribute to the progression of malignancy.[27,28] These results are similar to our ATAC-seq analysis, indicating that the key immune pathways were activated in hot tumors. In contrast, cold tumors could facilitate the progression of GC at both transcriptomic and genomic levels.

The claudin family consists of 27 members and plays a vital role in the formation, integrity, and function of tight junctions.[29] Claudin 3 is a member of the claudin family, and several studies have reported

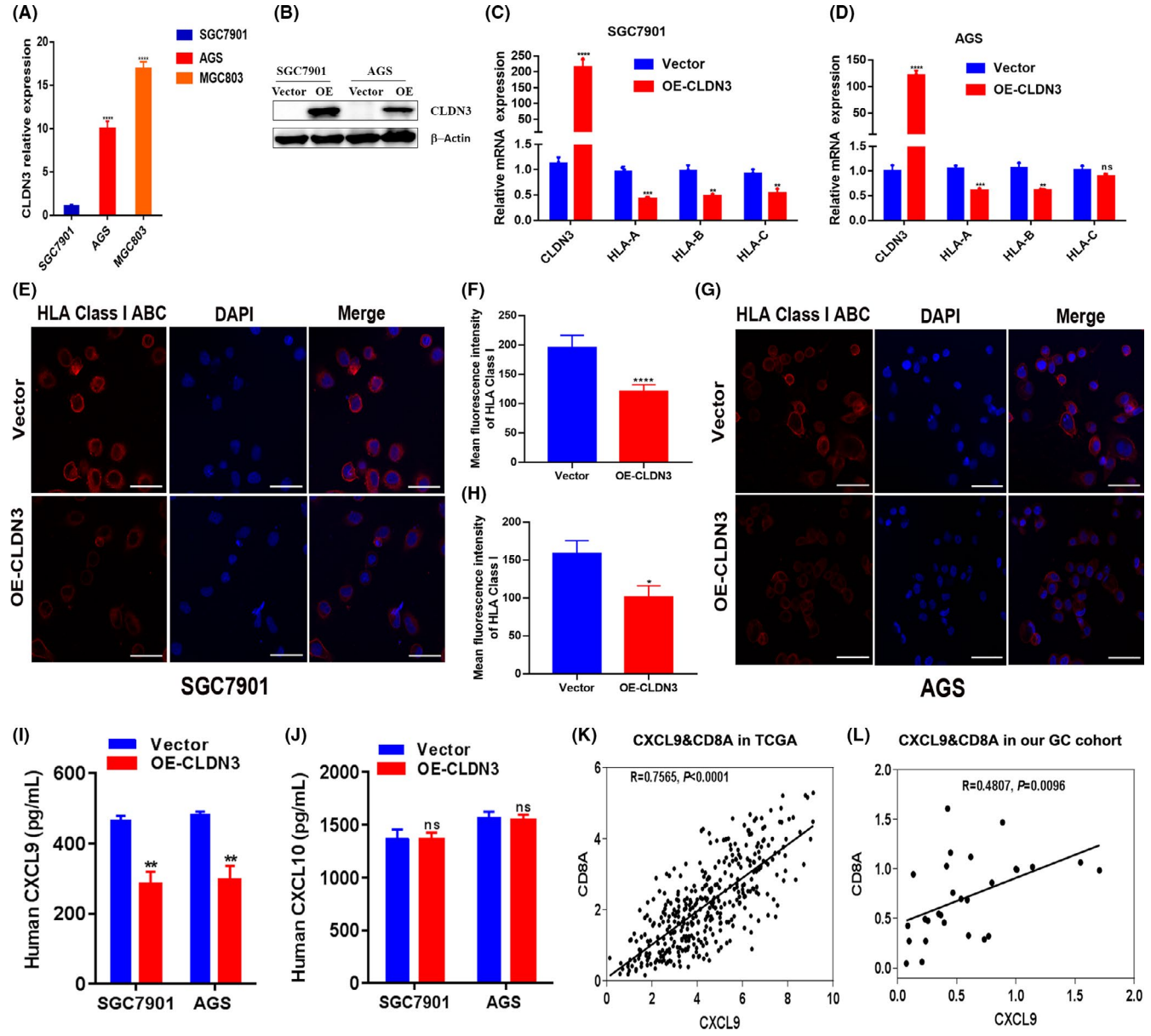

FIGURE 9 Claudin 3 (CLDN3) modulated the expression of MHC class I genes and the secretion level of CXCL9 in cancer cells. A, Relative expression levels of CLDN3 in three gastric cancer (GC) cell lines. B, Western blot analysis of CLDN3. C, D, Relative mRNA expression and (E-H) immunofluorescence of MHC-I in CLDN3-overexpressed (OE) and control cells (scale bar, 50 μm). I, J, ELISA for CXCL9 and CXCL10 in CLDN3-overexpressed cells. K, L, Correlation analysis of CXCL9 and CD8A expression in The Cancer Genome Atlas (TCGA) database and patient-derived GC samples (n = 28)

an association between CLDN3 and GC progression,[30,31] but the underlying mechanisms remained unclear. In the current study, CLDN3 was upregulated in cold tumors and negatively associated with immune cells in GC. In clinical samples CLDN3 was found to have negative correlation with $CD8^+$ T lymphocytes as well as CXCL9 and CXCL10, the chemokines which are vital for $CD8^+$ T lymphocyte recruitment.[32-34] Overexpression of CLDN3 did not affect the cell proliferation, cell colony formation, cell apoptosis, or cell wound healing in SGC7901 cells and AGS cells, suggesting that CLDN3 might not directly affect the biological function of GC cells; thus, it prompted us to explore the function of CLDN3 on the reprogramming of immune response in the TME of GC. As expected, overexpression of CLDN3 reduced the MHC-I expression in GC cells, indicating that CLDN3 could inhibit the immunogenicity of GC. Moreover, decreased levels of CXCL9 found in GC cells with upregulated CLDN3, clinical samples, and the TCGA dataset showed a positive correlation between CXCL9 and CD8A levels, suggesting that CLDN3 suppresses immune response by inhibiting $CD8^+$ T cell-related chemokines. In short, these findings favor the immunosuppressive role of CLDN3; thus, it could be a potential target of immunotherapy.

Several studies have used different prediction models to predict potential responses to immunotherapy, including the

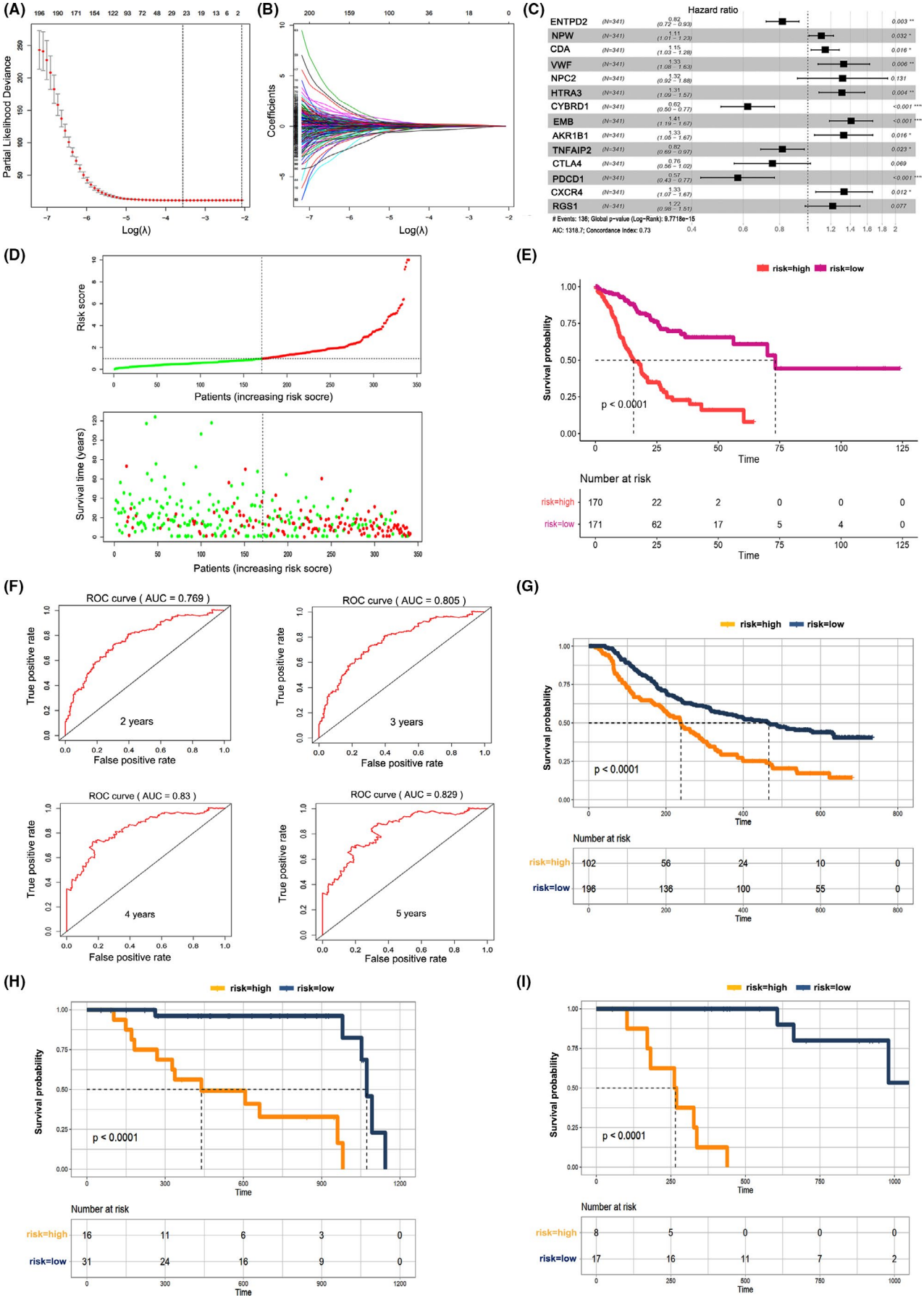
(A)
Partial Likelihood Deviance
Log(λ)
(B)
Coefficients
Log(λ)
(C)
Hazard ratio
ENTPD2 (N=341) 0.82 (0.72 − 0.93) 0.003 **
NPW (N=341) 1.11 (1.01 − 1.23) 0.032 *
CDA (N=341) 1.15 (1.03 − 1.28) 0.016 *
VWF (N=341) 1.33 (1.08 − 1.63) 0.006 **
NPC2 (N=341) 1.32 (0.92 − 1.88) 0.131
HTRA3 (N=341) 1.31 (1.09 − 1.57) 0.004 **
CYBRD1 (N=341) 0.62 (0.50 − 0.77) <0.001 ***
EMB (N=341) 1.41 (1.19 − 1.67) <0.001 ***
AKR1B1 (N=341) 1.33 (1.05 − 1.67) 0.016 *
TNFAIP2 (N=341) 0.82 (0.69 − 0.97) 0.023 *
CTLA4 (N=341) 0.76 (0.56 − 1.02) 0.069
PDCD1 (N=341) 0.57 (0.43 − 0.77) <0.001 ***
CXCR4 (N=341) 1.33 (1.07 − 1.67) 0.012 *
RGS1 (N=341) 1.22 (0.98 − 1.51) 0.077
Events: 136; Global p−value (Log−Rank): 9.7718e−15
AIC: 1318.7; Concordance Index: 0.73
(D)
Risk score
Patients (increasing risk socre)
Survival time (years)
Patients (increasing risk socre)
(E)
risk=high risk=low
Survival probability
p < 0.0001
Time
Number at risk
risk=high 170 22 2 0 0 0
risk=low 171 62 17 5 4 0
Time
(F)
ROC curve (AUC = 0.769)
True positive rate
2 years
False positive rate
ROC curve (AUC = 0.805)
3 years
ROC curve (AUC = 0.83)
4 years
ROC curve (AUC = 0.829)
5 years
(G)
risk=high risk=low
Survival probability
p < 0.0001
Time
Number at risk
risk=high 102 56 24 10 0
risk=low 196 136 100 55 0
(H)
risk=high risk=low
Survival probability
p < 0.0001
Time
Number at risk
risk=high 16 11 6 3 0
risk=low 31 24 16 9 0
(I)
risk=high risk=low
Survival probability
p < 0.0001
Time
Number at risk
risk=high 8 5 0 0 0
risk=low 17 16 11 7 2

FIGURE 10 Establishment and evaluation of clinical predictive models. A, B, LASSO regression method was used to search the hub immune signature. C, Multivariate Cox results of 14 hubs' immune signatures depicted by a forest plot. D, Distribution of risk score, recurrence status, and gene expression panel. E, Kaplan-Meier curves of overall survival in all patients with gastric cancer based on the risk score. F, Receiver operating characteristic (ROC) analysis of the predicting model for 2-, 3-, 4-, and 5-year risk in The Cancer Genome Atlas cohort. G-I, Kaplan-Meier survival curves for the anti-programmed cell death-1 treatment datasets between high- and low-risk groups

immunopredictive score (IMPRES) model for melanoma,[35] a neoantigen fitness model for melanoma and lung cancer,[36] and the immune-related risk score model for breast cancer.[37] However, the choice of effective prediction markers for GC immunotherapy is limited. Based on the DEGs between hot and cold tumors, we constructed a clinical prediction model related to immune infiltration, and to predict the OS of patients receiving immunotherapy. A large number of the genes in this model were closely related to the immune response. For example, *NPC2* is involved in the lipoprotein metabolism and innate immune signal pathways,[38] *ENTPD2* promotes differentiation of monocytic myeloid-derived suppressor cells into dendritic cells, and increase the efficacy of anti-PD-1/CTLA-4 immunotherapy.[39] *HTRA3* has been related to immune infiltration in GC and is critical for malignancy and prognosis.[40] Qin et al reported that cancer-associated fibroblasts affect cancer progression by affecting the CXCL12-CXCR4 axis in GC,[41] and upregulated *POU1F1* promoted GC metastasis by regulating macrophage polarization in a CXCL12/CXCR4-dependent manner.[42] *PDCD1* and *CTLA4* are the prognostic markers of immunotherapy. Overall, this model is highly reliable for the prognosis of OS and selecting suitable molecular markers for effective immunotherapy for GC.

In summary, we provided an in-depth analysis of the GC immune microenvironment. Our results revealed that the different molecular mechanisms of hot and cold tumors, both at the epigenomic and transcriptomic levels, suggest that hot tumors could alter chromatin accessibility and activate immune function-related pathways. However, cold tumors might induce epigenomic changes to promote tumorigenesis through both genome instability and shifts in transcription. In particular, we found that CLDN3 act as a key immune-suppressive modulator; targeting CLDN3 might reprogram cold into hot inflamed tumors, thus enhances the efficacy of tumor immunotherapy. In addition, a prediction model was constructed based on the differences in DEGs between hot and cold tumors to help clinicians in their routine clinical practice in the diagnosis and prognosis of GC patients and selecting appropriate targets for immunotherapy.

ACKNOWLEDGMENTS

This work was supported by the National Key Research and Development Program in China (No. 2020YFC2006100), Excellent Foreign Scientist Studio of Henan Province in China (No. GZS2018001), Zhengzhou Major Collaborative Innovation Project (No. 18XTZX12003), key projects of discipline construction in Zhengzhou University (No. XKZDJC202001), and medical service capacity improvement project of Henan Province in China (grant Yu Wei Medicine [2017] No. 66).

CONFLICT OF INTEREST

The authors have no conflicts of interest.

ETHICAL APPROVAL

This study has been approved by the Ethics Committee of the Fifth Affiliated Hospital of Zhengzhou University (KY2020029), and informed consent was obtained from all participants. All the sampling and experimental procedures were carried out by strictly following the guidelines of the Helsinki Declaration of 1964 and its latest amendments.

DATA AVAILABILITY STATEMENT

The raw data supporting the conclusions of this article will be available from the corresponding author with a reasonable request.

ORCID

Bin Liu https://orcid.org/0000-0002-1336-8387
Pengyuan zheng https://orcid.org/0000-0003-1647-0253
Yang Mi https://orcid.org/0000-0003-2905-4830

REFERENCES

1. Siegel RL, Miller KD, Jemal A. Cancer statistics, 2020. *CA Cancer J Clin*. 2020;70:7-30.
2. Arnold M, Abnet CC, Neale RE, et al. Global burden of 5 major types of gastrointestinal cancer. *Gastroenterology*. 2020;159:335–349.e15d.
3. Taieb J, Moehler M, Boku N, et al. Evolution of checkpoint inhibitors for the treatment of metastatic gastric cancers: Current status and future perspectives. *Cancer Treat Rev*. 2018;66:104-113.
4. Stein A, Moehler M, Trojan J, Goekkurt E, Vogel A. Immuno-oncology in GI tumours: clinical evidence and emerging trials of PD-1/PD-L1 antagonists. *Crit Rev Oncol Hematol*. 2018;130:13-26.
5. Abozeid M, Rosato A, Sommaggio R. Immunotherapeutic strategies for gastric carcinoma: a review of preclinical and clinical recent development. *Biomed Res Int*. 2017;2017:5791262.
6. Galon J, Bruni D. Approaches to treat immune hot, altered and cold tumours with combination immunotherapies. *Nat Rev Drug Discov*. 2019;18:197-218.
7. Haanen J. Converting cold into hot tumors by combining immunotherapies. *Cell*. 2017;170:1055-1056.
8. Pages F, Mlecnik B, Marliot F, et al. International validation of the consensus Immunoscore for the classification of colon cancer: a prognostic and accuracy study. *Lancet*. 2018;391:2128-2139.
9. Mariathasan S, Turley SJ, Nickles D, et al. TGFbeta attenuates tumour response to PD-L1 blockade by contributing to exclusion of T cells. *Nature*. 2018;554:544-548.
10. Riaz N, Havel JJ, Makarov V, et al. Tumor and microenvironment evolution during immunotherapy with nivolumab. *Cell*. 2017;171:934–949.e16.
11. Hugo W, Zaretsky JM, Sun L, et al. Genomic and transcriptomic features of response to anti-PD-1 therapy in metastatic melanoma. *Cell*. 2016;165:35-44.

12. Corces MR, Granja JM, Shams S, et al. The chromatin accessibility landscape of primary human cancers. *Science*. 2018;362:eaav1898.
13. Aran D, Hu Z, Butte AJ. xCell: digitally portraying the tissue cellular heterogeneity landscape. *Genome Biol*. 2017;18:220.
14. Aran D. Cell-type enrichment analysis of bulk transcriptomes using xcell. *Methods Mol Biol*. 2020;2120:263-276.
15. Tamborero D, Rubio-Perez C, Muinos F, et al. A pan-cancer landscape of interactions between solid tumors and infiltrating immune cell populations. *Clin Cancer Res*. 2018;24:3717-3728.
16. Li T, Fan J, Wang B, et al. TIMER: a web server for comprehensive analysis of tumor-infiltrating immune cells. *Cancer Res*. 2017;77:e108-e110.
17. Kraft M, Riedel S, Maaser C, et al. IFN-gamma synergizes with TNF-alpha but not with viable *H. pylori* in upregulating CXC chemokine secretion in gastric epithelial cells. *Clin Exp Immunol*. 2001;126:474-481.
18. Turley SJ, Cremasco V, Astarita JL. Immunological hallmarks of stromal cells in the tumour microenvironment. *Nat Rev Immunol*. 2015;15:669-682.
19. Salmon H, Franciszkiewicz K, Damotte D, et al. Matrix architecture defines the preferential localization and migration of T cells into the stroma of human lung tumors. *J Clin Invest*. 2012;122:899-910.
20. Zhang M, Daniel S, Huang Y, et al. Anti-West Nile virus activity of in vitro expanded human primary natural killer cells. *BMC Immunol*. 2010;11:3.
21. Robertson MJ, Ritz J. Biology and clinical relevance of human natural killer cells. *Blood*. 1990;76:2421-2438.
22. Jaigirdar SA, MacLeod MK. Development and function of protective and pathologic memory CD4 T cells. *Front Immunol*. 2015;6:456.
23. Nissim Ben Efraim AH, Levi-Schaffer F. Roles of eosinophils in the modulation of angiogenesis. *Chem Immunol Allergy*. 2014;99:138-154.
24. Varricchi G, Galdiero MR, Loffredo S, et al. Eosinophils: The unsung heroes in cancer? *Oncoimmunology*. 2018;7:e1393134.
25. Lee YH, Martin-Orozco N, Zheng P, et al. Inhibition of the B7–H3 immune checkpoint limits tumor growth by enhancing cytotoxic lymphocyte function. *Cell Res*. 2017;27:1034-1045.
26. Picarda E, Ohaegbulam KC, Zang X. Molecular pathways: targeting B7–H3 (CD276) for human cancer immunotherapy. *Clin Cancer Res*. 2016;22:3425-3431.
27. Blumenthal RD, Hansen HJ, Goldenberg DM. Inhibition of adhesion, invasion, and metastasis by antibodies targeting CEACAM6 (NCA-90) and CEACAM5 (Carcinoembryonic Antigen). *Cancer Res*. 2005;65:8809-8817.
28. Kakugawa S, Langton PF, Zebisch M, et al. Notum deacylates Wnt proteins to suppress signalling activity. *Nature*. 2015;519:187-192.
29. Turksen K, Troy TC. Junctions gone bad: claudins and loss of the barrier in cancer. *Biochim Biophys Acta*. 2011;1816:73-79.
30. Matsuda Y, Semba S, Ueda J, et al. Gastric and intestinal claudin expression at the invasive front of gastric carcinoma. *Cancer Sci*. 2007;98:1014-1019.
31. Zhang Z, Yu W, Chen S, Chen Y, Chen L, Zhang S. Methylation of the claudin3 promoter predicts the prognosis of advanced gastric adenocarcinoma. *Oncol Rep*. 2018;40:49-60.
32. Koelink PJ, Overbeek SA, Braber S, et al. Targeting chemokine receptors in chronic inflammatory diseases: an extensive review. *Pharmacol Ther*. 2012;133:1-18.
33. Parsonage G, Machado LR, Hui JW, et al. CXCR6 and CCR5 localize T lymphocyte subsets in nasopharyngeal carcinoma. *Am J Pathol*. 2012;180:1215-1222.
34. Oldham KA, Parsonage G, Bhatt RI, et al. T lymphocyte recruitment into renal cell carcinoma tissue: a role for chemokine receptors CXCR3, CXCR6, CCR5, and CCR6. *Eur Urol*. 2012;61:385-394.
35. Auslander N, Zhang G, Lee JS, et al. Robust prediction of response to immune checkpoint blockade therapy in metastatic melanoma. *Nat Med*. 2018;24:1545-1549.
36. Luksza M, Riaz N, Makarov V, et al. A neoantigen fitness model predicts tumour response to checkpoint blockade immunotherapy. *Nature*. 2017;551:517-520.
37. Wang S, Xiong Y, Zhang Q, et al. Clinical significance and immunogenomic landscape analyses of the immune cell signature based prognostic model for patients with breast cancer. *Brief Bioinform*. 2020;22:1-15.
38. Wei D, Shen S, Lin K, et al. NPC2 as a Prognostic Biomarker for Glioblastoma Based on Integrated Bioinformatics Analysis and Cytological Experiments. *Front Genet*. 2021;12:611442.
39. Chiu DK, Tse AP, Xu IM, et al. Hypoxia inducible factor HIF-1 promotes myeloid-derived suppressor cells accumulation through ENTPD2/CD39L1 in hepatocellular carcinoma. *Nat Commun*. 2017;8:517.
40. Ji C, Sun LS, Xing F, et al. HTRA3 Is a prognostic biomarker and associated with immune infiltrates in gastric cancer. *Frontiers in oncology*. 2020;10:603480.
41. Qin Y, Wang F, Ni H, et al. Cancer-associated fibroblasts in gastric cancer affect malignant progression via the CXCL12-CXCR4 axis. *J Cancer*. 2021;12:3011-3023.
42. Tang C, Lei X, Xiong L, Hu Z, Tang B. HMGA1B/2 transcriptionally activated-POU1F1 facilitates gastric carcinoma metastasis via CXCL12/CXCR4 axis-mediated macrophage polarization. *Cell Death Dis*. 2021;12:422.

SUPPORTING INFORMATION

Additional supporting information may be found online in the Supporting Information section.

How to cite this article: Ren F, Zhao Q, Zhao M, et al. Immune infiltration profiling in gastric cancer and their clinical implications. *Cancer Sci*. 2021;112:3569–3584. https://doi.org/10.1111/cas.15057